ION CHANNELS, RECEPTORS AND TRANSPORTERS

Malformation of junctional microdomains in cataract lens membranes from a type II diabetes patient

Stéphanie Mangenot · Nikolay Buzhynskyy ·
Jean-François Girmens · Simon Scheuring

Abstract In eye core lens membranes, aquaporin-0 (AQP0) and connexins (Cx) form together well-structured supramolecular assemblies, the junctional microdomains, in which they assure water, ion, metabolite, and waste transport. Additionally, they mediate cell–cell adhesion-forming thin junctions (AQP0) and gap junctions (Cx). We have used atomic force microscopy and biochemical methods to analyze and compare the structure of junctional microdomains in human cataract lens membranes from a type II diabetes patient and healthy lens membranes from calf. A healthy intercellular junctional microdomain consists in average of ~150 tetragonally arranged ($a=b=65.5$ Å, $\gamma=90°$) AQP0 tetramers surrounded by densely packed non-ordered connexon channels. Gap-junction connexons act as lineactants inside the membrane and confine AQP0 in the junctional microdomains. In the diabetic cataract lens, connexons were degraded, and AQP0 arrays are malformed. We conceptualize that absence of connexons lead to breakdown of cell nutrition.

S. Mangenot · N. Buzhynskyy · S. Scheuring (✉)
Institut Curie, Équipe INSERM Avenir, UMR168-CNRS,
26 Rue d'Ulm,
75248 Paris Cedex 05, France
e-mail: simon.scheuring@curie.fr

S. Mangenot
Université Paris-Sud,
15 Rue Georges Clémenceau,
91405 Orsay Cedex, France

J.-F. Girmens
Centre Hospitalier National d'Ophtalmologie des Quinze-Vingts,
Service IV & CIC,
28 rue de Charenton,
75571 Paris Cedex 12, France

Introduction

The mammalian eye lens [1] has developed some remarkable adaptations to assure transparency and to change shape for focusing on different distances (accommodation) [2]: To minimize light scattering, the lens is avascular. Furthermore, lens cells have degraded organelles during differentiation and contain a high concentration of crystallin proteins [3]. The cells are tightly packed to make intercellular distances smaller than the wavelength of visible light. To explain how cells that have degraded their organelles and are located deeply inside the lens are nourished, an internal microcirculation model was proposed that maintains a flow of water - ions, and metabolites [2]: solutes flow in the extracellular space, enter deeper-lying lens cells, and flow through cell-to-cell channels back toward the lens periphery. Two types of membrane proteins form cell-to-cell junctions assuring metabolite transport, ion transport, waste evacuation, water homeostasis and adhesion between fiber cells: lens-specific aquaporin-0 (AQP0) [4, 5] and gap-junction connexins (Cx) [6]. Mutations in both proteins result in the formation of cataract [7].

Cataracts are opacifications of eye lenses that lead to blindness and affect about two thirds of the population over 65 years; surgery is the only cure. Therefore, the importance of cataract care is increasing with the rise of worldwide population and age. Besides age, recognized risk factors are long-term ultraviolet exposure and exposure to radiation. Cataracts can also develop as secondary effects of diseases such as diabetes and hypertension, among others. Notably,

type II diabetes, also called non-insulin-dependent diabetes, provoked by excess body weight or physical inactivity, prevalent in developed countries [8], is projected to rise from 171 million in 2000 to 366 million in 2030 [9].

The atomic force microscope (AFM [10]) has become powerful in membrane research. It has been successfully used to image membrane protein 2D-crystals [11], densely packed reconstitution [12], and native membranes [13]. High-resolution AFM has been used to analyze the supramolecular membrane protein assembly of several purple bacteria species [13–19]. Studies of eukaryotic native membranes are rare. The rod outer segment membranes comprising rhodopsin as single component have been imaged [20], as well as studies of the supramolecular assembly of ATP synthases and the voltage-gated anion channel (VDAC) in the inner and outer mitochondrial membranes, respectively [21, 22]. So far, the only work-presenting high-resolution AFM images on a multicomponent mammalian membrane has elucidated the organization of junctional microdomains composed of AQP0 square arrays surrounded by gap-junction connexons in sheep lens core cell membrane [23]. This work built the basis for structural models [24]. The AFM can be operated under medical relevant conditions (ambient temperature and pressure in physiological buffer solution), allowing studying tissue debris obtained through surgery. Recently, we described senile human cataract lens membranes that revealed junctional microdomains of full-length and truncated AQP0 and a lack of connexins [25].

In the present study, we used AFM and unveiled the junctional microdomain organization and structure of a pathological human tissue, the cataract eye lens membranes from a type II diabetes patient at unprecedented submolecular resolution. In healthy calf and sheep lens junctional microdomains, connexons function as lineactants that confine AQP0 arrays. In the cataract lens, connexons are absent at borders of junctional microdomains leading to malformation of the AQP0 arrays and possibly breakdown of the lens microcirculation system.

Results and discussion

The supramolecular assembly of membrane channels in healthy lens membranes

We have acquired in a previous high-resolution AFM study a clear-cut picture of the junctional microdomain architecture in sheep [23]. Here we additionally assessed the supramolecular assembly of junctional microdomains in healthy younger lenses from calf, providing additional insights to the maturation of the lens compared to the adult sheep tissue studied before [23]. Purified lens membranes from fiber cells were adsorbed to freshly cleaved mica. The soft

purification method did not separate the adjacent membranes of thin junctions. Using the AFM tip as a nano-dissector, the top membranes were removed [23], thus allowing to record high-resolution topographs of the extracellular interface of the junctional microdomains. Membranes display characteristic square AQP0 arrays (Fig. 1a,b) with a lattice of $a=b=65.5\pm0.5$ Å and $\gamma=90°\pm1°$. To analyze long-range array characteristics, we calculated the pair-correlation function (PCF) of AQP0 arrays (Fig. 1c). Beyond the characteristic $r=65.5$ Å peak, we find long-range peaks, corresponding to AQP0 neighbors located at distances $\sqrt{2}r=92.6$ Å, $2r=131$ Å, $\sqrt{5}r=146.5$ Å and so on. These higher-order peaks are the signature of a good crystallin order, their broadening reports about weak lattice distortions, and the distance r when the PCF is <1 ($r\sim400$ Å) documents the array edge distance (~800 Å in diameter). At high-resolution (≤2.5 Å/pixel) individual surface protruding loops are visible in the raw data topograph (Fig. 1d). We found, so far, unreported screw dislocations of AQP0 in some arrays (Fig. 1e). AQP0 tetramers are shifted by approximately half of a unit, leading to a "zipper-like" arrangement. This mismatch in the supramolecular assembly is energetically unfavorable. Moreover, such defaults persisted and were observed over long time periods (>1 h). If AQP0s were able to move inside the array, they would correct this default to fill the energetic gap. As this is not the case, we conclude that AQP0 are diffusion immobile in the arrays.

The AQP0 average topography highlights the details detectable by AFM, i.e., individual helix-connecting loops (Fig. 1f). In particular, the exposed proline-rich domains of loops A and C responsible for junction formation [26] of each monomer are clearly visible. The AQP0 standard deviation (SD) map (Fig. 1g) reveals that the central loop A is as flexible as peripheral loop C, whose topography is predominant. This observation reflects the flexibility of

Fig. 1 High-resolution AFM analysis of AQP0 in junctional microdomains of healthy lens membranes. **a**, **b** AQP0 form square lattices over large areas. Rarely AQP0 lattices are invaded by other molecules (**a**), or AQP0 rows are out of register (**b**, *arrowheads*). **c** Pair correlation function (PCF) analysis of AQP0 arrays (lattice dimensions: $a=b=65.5$ Å±1 Å, $\gamma=90°\pm1°$) shown in (**a**) and (**b**). The PCF analysis peaks first at 65.5 Å, and features longer distance peaks at ~95 Å ($\sqrt{2}\cdot65.5$Å) and multiples of the lattice dimensions (~131 Å). **d**, **e** High-resolution scans (2.5 Å/pixel) of (**a**) and (**b**). Individual surface protruding loops are visible (**d**, *arrowheads*). Out-of-register AQP0 *rows* are in a *zipper-like arrangement* with displacements of approximately half the unit cell dimension (**e**, *outlines*). **f** AQP0 average topography (full color scale: 4 Å < height < 14 Å). **g** Standard deviation map (full color scale: 0.2 Å < SD < 1.1 Å). The two peripheral protrusions house the beginning (residues: Pro 109, Pro 110, Ala 111 and Val 112) and the end of extracellular loop C (residues: His 122, Pro 123, Gly 124, and Val 125). The third protrusion close to the center of the tetramer represents loop A (residues: Ala 35, Pro 36, Gly 37, and Pro 38). Loop A is particularly flexible: its average topography is lower than loop C (**f**), but its SD values are similar (**g**). **h** Structural model of the AQP0 assembly
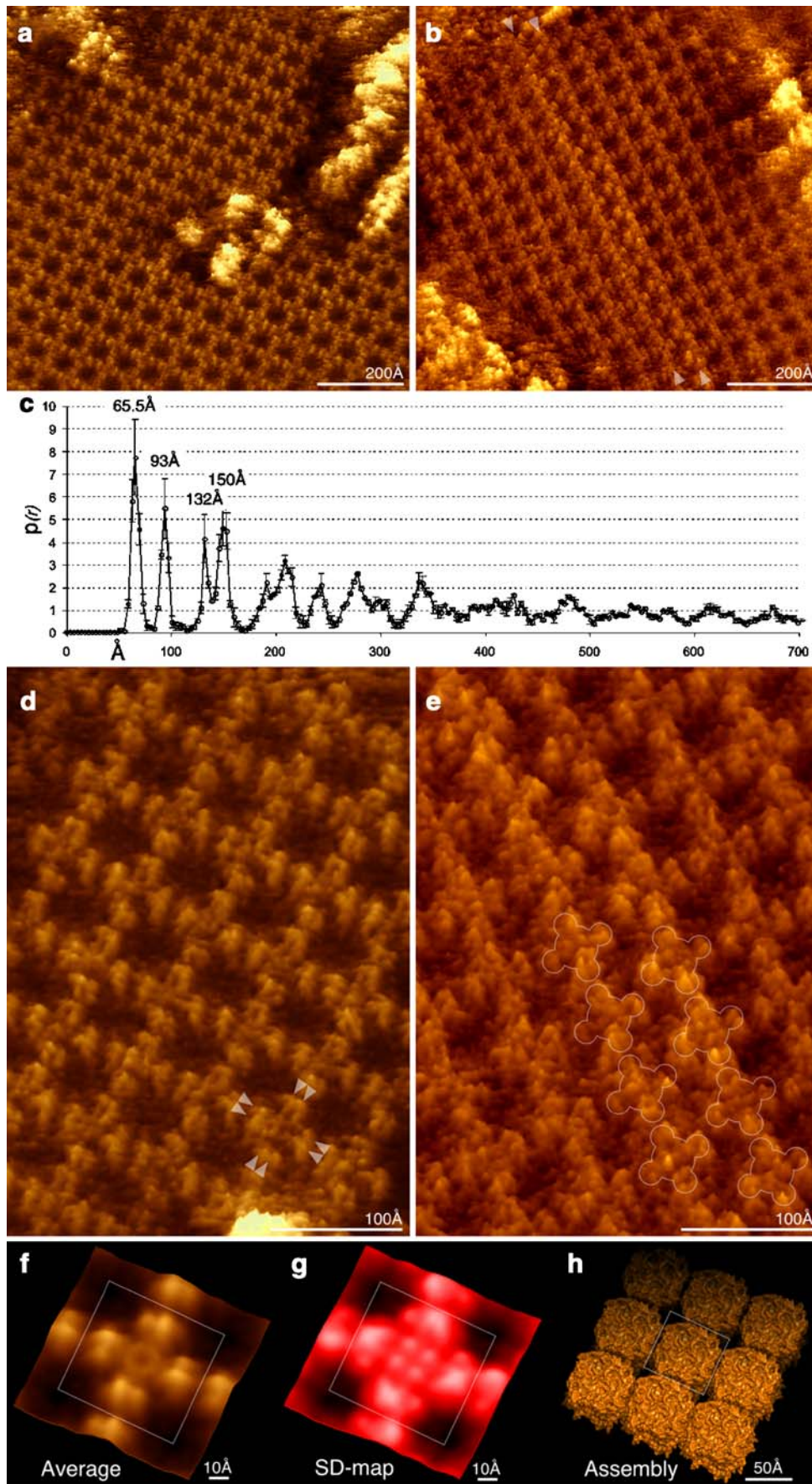
loop A, which occupies different locations in the open and closed AQP0 structures [26, 27]. A space-filling model of the native AQP0 organization (Fig. 1h) based on lattice determination and PCF analysis shows that the space for lipid molecules between AQP0 tetramers is available, as found in the 2D crystals [28].

Overview images of healthy lens membranes (Fig. 2a) showed the presence of multiple differently oriented arrays that were surrounded by non-ordered and strongly corrugated proteins [23]. These proteins confined and separated

AQP0 arrays (Fig. 2b). They protruded more from the membrane than AQP0 and were flower-shaped molecules with ~70 Å in diameter in agreement with the dimension of connexons, the second most abundant membrane protein in lenses [6, 23]. Although these molecules were more difficult to image than AQP0, high-resolution AFM topographs (Fig. 2c) have been used to compute averages identifying them unambiguously as connexons (Fig. 2d). Profile analysis of connexons displayed a protrusion height of 12 Å above the AQP0 array (full height of 22 Å above
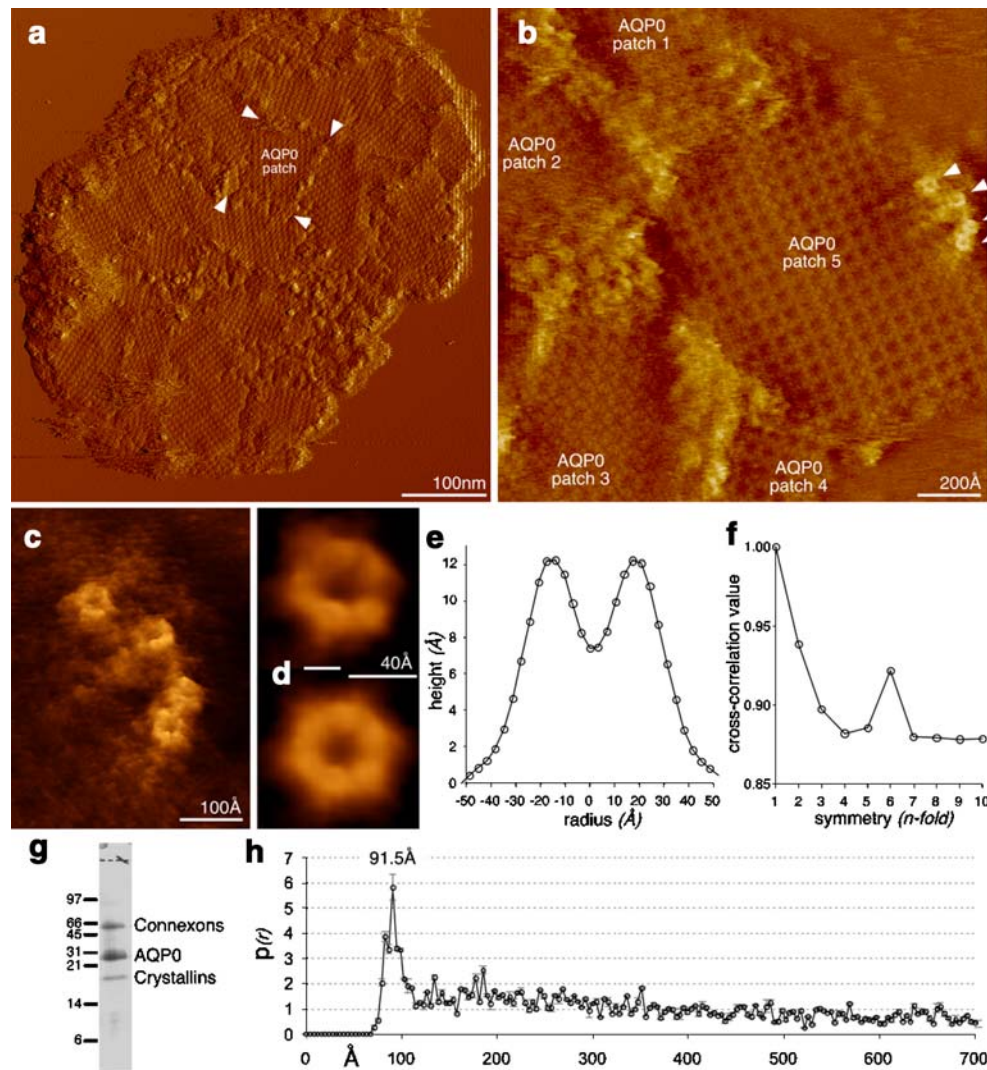
Fig. 2 The junctional microdomains in healthy calf lens core membranes. **a** Overview deflection image revealing multiple differently oriented AQP0 arrays associated. Often, individual AQP0 arrays are surrounded by rows of molecules that are more strongly corrugated than the square-patterned AQP0 array in the center (*arrowheads*). **b** High-resolution topograph showing five individual and differently oriented AQP0 arrays separated and edged by stronger protruding connexons (*arrowheads*). **c** Perspective view (15° tilted) of four individual connexons at the edge of an AQP0 array shown in (**b**). **d** Non-symmetrized (*top*) and symmetrized (*bottom*) connexon average of molecules shown in (**c**). **e** Average radial plot analysis of connexons. Diameter: ~70 Å, top diameter: ~50 Å, central pore diameter ~20 Å. **f** Symmetry analysis of the non-symmetrized connexon average (**d**, *top*) peaks at sixfold symmetry. **g** SDS-PAGE analysis of the calf lens membranes. Three major bands were detected at ~60, ~28, and ~18 kDa, attributed to connexons, AQP0, and crystallins. The AQP0 band is approximately twice as strong as the connexon band. **h** Pair correlation function (PCF) analysis of connexons in native sheep junctional microdomains. The PCF analysis peaks at 91.5 Å, and features, due to the absence of order between connexon channels no significant long-range peaks

the bilayer), a central channel cavity with ~20 Å diameter, and outer and top diameters of ~70 and ~50 Å, respectively (Fig. 2e). Symmetry analysis of the average revealed sixfold symmetry (Fig. 2f). Shape, symmetry, and dimensions are in good agreement with the electron microscopy structure of connexons [29]. Sodium dodecyl sulfate polyacrylamide gel electrophoresis (SDS-PAGE) analysis (Fig. 2g) corroborated the abundance of aquaporins and connexins. A low molecular weight protein band was attributed to crystallins [30], which have a molecular weight of about 21 kDa and are known to interact with AQP0 on the membrane surface [31]. Contrary to the crystallin AQP0 arrays, PCF analysis reveals that connexons in sheep [23] and calf are non-ordered and sparsely packed, with an average intermolecular distance of ~91.5 Å [23]. Connexons have no long-range order, as documented by the single peak in the PCF analysis. AQP0 arrays are thus surrounded and confined by a few rows of non-ordered connexons. The colocalization and specificity of interaction between AQP0 and connexons have been shown by immunofluorescence and immunoprecipitation experiments [32]. Interestingly, the supramolecular structure of junctional microdomains and the localization of connexons are very similar in young lenses from calf and mature lenses from sheep. However, in the young tissue, full-length AQP0 is predominant (Fig. 2g), while in mature lenses, about 50% of AQP0 is truncated [23]. This is strong evidence that the supramolecular structure of junctional microdomains does not depend on AQP0 truncation and that the supramolecular organization of junctional microdomains in healthy eye lens fiber cells is formed at an early stage of eye development. While we have no access to healthy human lenses, we use ovine and bovine lenses for comparison with the pathological human case. Sequence identity and similarity between human and sheep AQP0 is 92.4% and 98.9%, respectively, and between human and bovine AQP0, it is 92.0% and 98.5%, respectively. It can be assumed that the architecture and function of junctional microdomains is shared among mammal eye lenses [1, 33].

The cataract lens membranes of the type II diabetes patient lack connexons

In contrast to our analysis of the healthy state, where we investigated material from 20 lenses, we were interested in characterizing one individual pathological lens. This nanomedical approach allows the acquisition of relevant information about the pathology of a patient at the single molecule level. In this study, membranes from cataract eye lens surgery debris of the right eye of a type II diabetes patient with preoperative visual acuity of 1/10 were analyzed. Overview image analysis revealed large lipid bilayer membranes containing oddly dispersed junctional microdomains of

rectangular shape (Fig. 3a). Indeed, the AQP0 tetramers were arranged in junctional microdomains whose borders were badly defined and revealed a fuzzy appearance (Fig. 3b). Single rows of individual AQP0 tetramers as well as patches composed of two or three rows were found besides large arrays. Such dislocations of individual tetramers were never observed in healthy lens membranes. It is questionable whether such AQP0 microdomains can still form stable platforms for thin-junction formation with neighboring cells. It is clear that a lineactant that confines and defines the shape
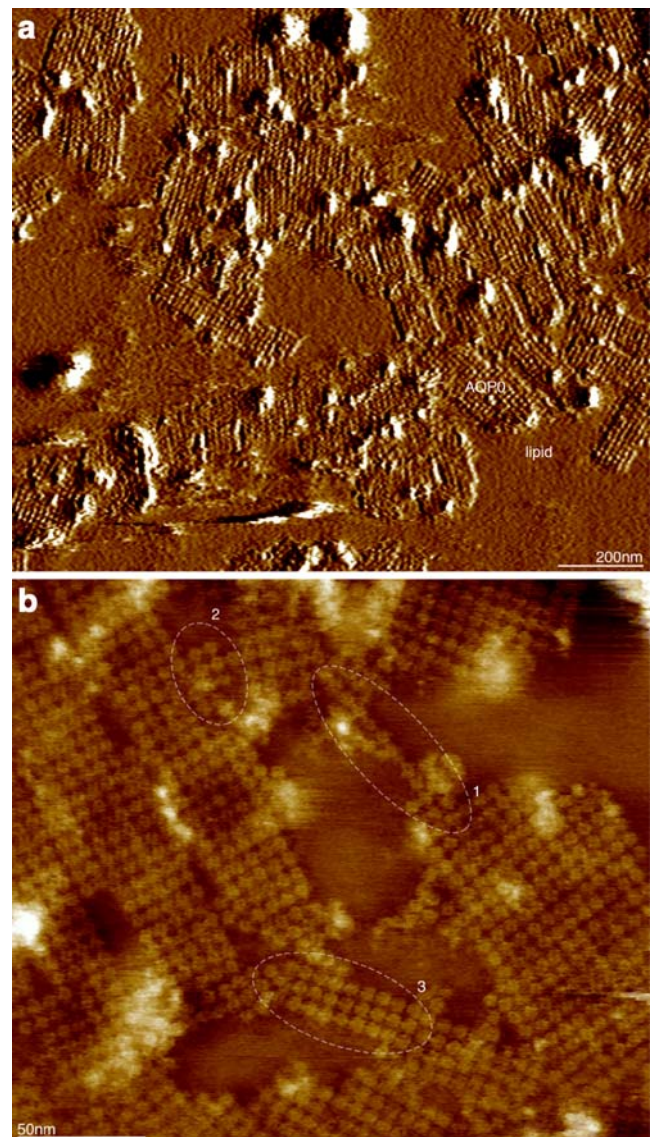
Fig. 3 AFM analysis of cataract lens membranes from a type II diabetes patient. **a** Large smooth lipid membranes contain the junctional microdomains that appear as corrugated domains. **b** In the diabetes II cataract membranes, the square AQP0 patches are not surrounded by connexons, and the patch suprastructure appears more fuzzy than in the native case (compare with Fig. 1). AQP0 tetramers are found in single rows (*outline 1*), rows of 2 (*outline 2*), 3 (*outline 3*) or many, the AQP0 tetramer is hence the base unit of the AQP0 array assembly

and boarders of the junctional microdomains is missing in the type II diabetes cataract case. Indeed, we could never image connexons neither at the edges of AQP0 arrays nor elsewhere in the cataract sample. Our findings show the power of the AFM for imaging single molecules in a tissue originating from surgery. No other technique could reveal the single molecule disorder of AQP0 at array edges or the absence of connexons at this location.

It is important to note that we have used the same membrane preparation method for healthy calf and sheep and the cataract surgery debris, except for the preceding phacoemulsification step used to remove the lens from the patient's eye. Anyway, phacoemulsification results in millimeter-sized tissue debris containing cell ensembles. We therefore think that the membrane organization is preserved. As the supramolecular assembly of membrane proteins in the healthy cases resemble previous electron microscopy studies [33, 34], we are confident that the alteration observed in the cataract case are relevant.

AFM single molecule imaging of membranes of a type II diabetes patient cataract revealed the absence of connexons in the pathological case, in contrast to the connexons found in the intact calf lens membranes. In order to backup and assert the AFM data, we performed MALDI-TOF (Fig. 4a,b) and SDS-PAGE (Fig. 4c) analyses of the cataract-originating membranes. Both experiments attested the presence of full-length AQP0(L263) with a mass of 28,100±60 Da and of truncated AQP0(S245) with a mass of 26,370±60 Da. Our

mass measurements suggested most frequent C-terminal cleavage of the human AQP0 sequence (Fig. 4d) at Serine (245) [35]. A minor peak in the MALDI-TOF spectrum at a molecular mass of ~20,000 Da was attributed to tetraspanin [36], whereas the ~21,000 Da peak corresponded to proteins of the crystallin family [30] that were shown to interact with AQP0 at the membrane surface [31]. No MALDI-TOF peak and no SDS-PAGE band attributable to connexons were found.

We statistically compared the morphology of 34 and 45 junctional microdomains from a preparation containing 20 native calf lenses and from an individual cataract lens of the type II diabetes patient, respectively (Fig. 5). The sizes of the microdomains in intact and diabetic cataract membranes were similar containing ~150 AQP0 tetramers per array (Fig. 5a), and in both cases, the relative orientations of the arrays were random (Fig. 5b). In contrast, the microdomains were more round and homogenous in the healthy than in the pathological case, probably due to the presence of the connexons that function as lineactants around the aquaporin arrays (Fig. 5c). Moreover, the fuzzy offshoots of only a few AQP0 tetramers detaching from the arrays were statistically difficult to assess, but were representative for the odd-defined supramolecular assembly of the pathological junctional microdomains (see also Fig. 3). The presence and absence of connexons at the edges of junctional microdomains in the healthy and the pathological membranes, respectively, was the crucial difference between the two
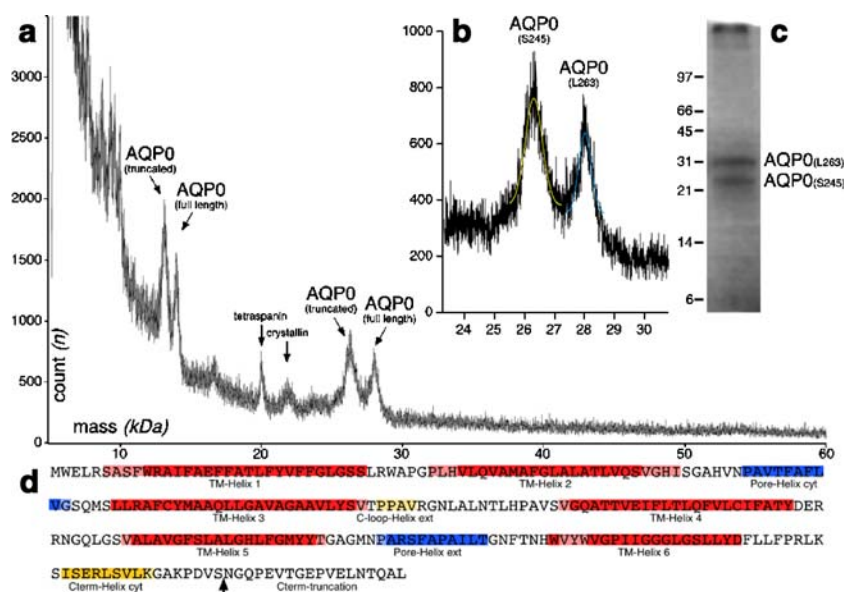
Fig. 4 MALDI-TOF analysis of cataract lens membranes from a type II diabetes patient. a Major peaks for single and double ionized full-length and truncated AQP0 were found. No peak was detected between 40 and 60 kDa that could account for the most abundant connexons C×43, C×45 and C×50 in human. b Full-length and truncated AQP0 were identified as AQP0(L263) and AQP0(S245) with masses of 28,100±60 Da and of 26,370±60 Da, respectively. c

SDS-PAGE analysis equally identified two proteins of mass corresponding to full-length and truncated AQP0, and no higher-mass protein. d Sequence of human AQP0. The transmembrane helix regions are shaded in red, the pore loops in blue, and extramembraneous helices in yellow. The most frequent truncation site (S245) is indicated by the arrow
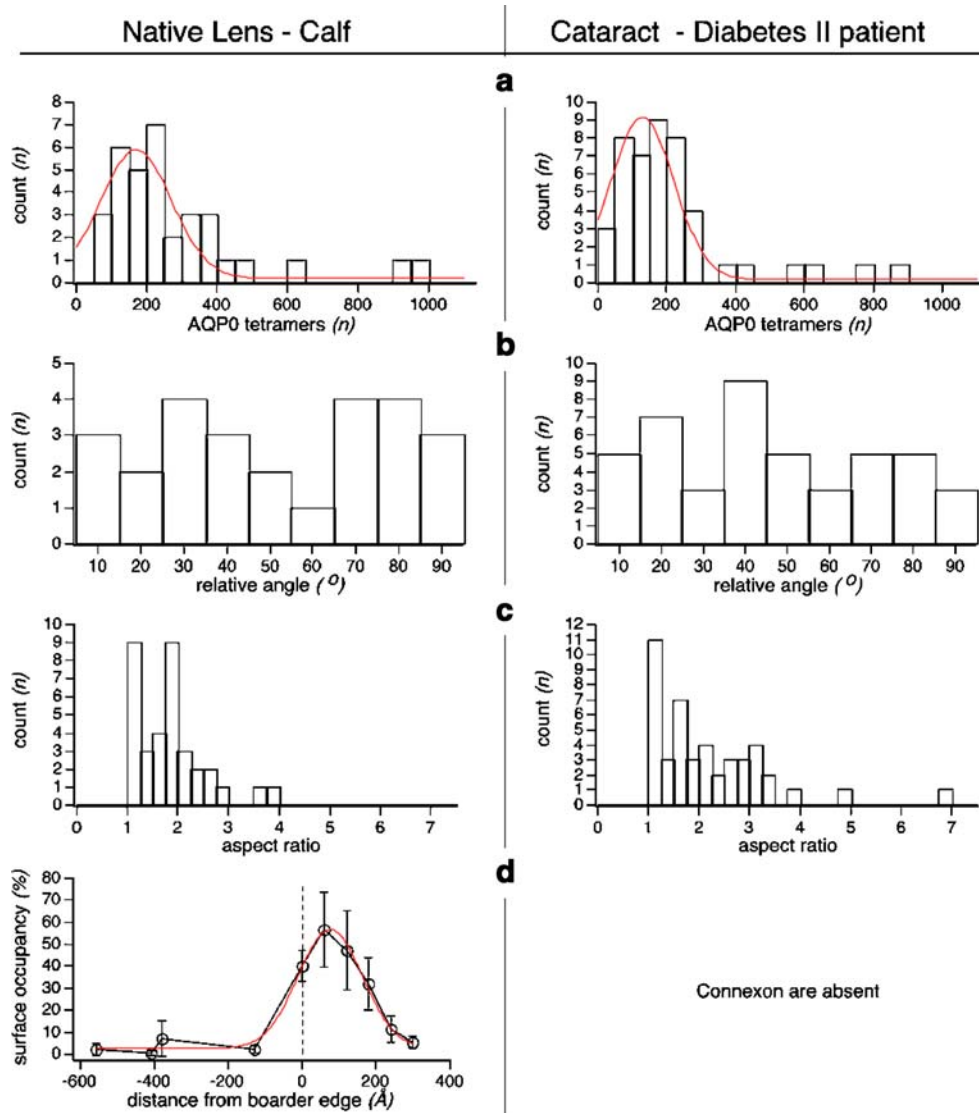
Fig. 5 Analysis of junctional microdomain morphology in the native lens and the diabetes II patient cataract membranes. **a** Histogram analyses of the number of AQP0 tetramers per individual array in the native (*left*) and in the type II diabetes cataract (*right*) lens membrane. The native and the pathological AQP0 arrays are similar in size, 170 ± 70 versus 130 ± 60 AQP0 tetramers (peak position±half width at full height), respectively. **b** Relative orientation (with respect to the image X-axis) of the AQP0 arrays in the native (*left*) and in the type II diabetes cataract (*right*) lens membranes. The native and the pathological AQP0 arrays orientation appears stochastic and arbitrary, $50°\pm27°$ versus $46°\pm24°$ (average±SD), respectively. **c** Aspect ratio of the AQP0 arrays in the native (*left*) and in the type II diabetes cataract (*right*) lens membranes. The native junctional microdomains are more roundish and homogeneous in shape than the pathological ones, 1.8 ± 0.6 versus 2.2 ± 1.1 (average±SD), respectively. Furthermore, in the type II diabetes cataract lens membranes, AQP0 arrays branch out into rows of few AQP0 tetramers (compare Figs. 1 and 3). **d** Connexon repartition analysis around the AQP0 array boarder. Connexon occupancy is highest (~60% of the surface area) at $75\text{Å}\pm120\text{Å}$ (peak position±half width at full height) outside the AQP0 array. In cataract lens membranes from the type II diabetes patient connexons are absent

samples. In the healthy case, connexon surface occupancy around the junctional microdomains was highest at ~75 Å distance from the AQP0 array edge (Fig. 5D). This distance is intermediate compared to the AQP0–AQP0 intermolecular distance (65.5 Å, see Fig. 1) and the connexon–connexon intermolecular distance (91.5 Å, see Fig. 2) and, therefore, accounts for both half distances in an AQP0–connexon assembly that is loosely packed. Very rarely, connexons are integrated in AQP0 arrays.

In conclusion, eye lens junctional microdomains consisted in average of ~150 AQP0 tetramers that were arranged in a compact square lattice of 65.5 Å. In the pathological case, the microdomains were malformed, distorted, and branch out in rows of individual AQP0. We think that this is the

consequence of the absence of connexons that act as lineactants in the two-dimensional membrane confining the AQP0 arrays in the healthy case. The lineactant function of connexons is a novel proposal. However, the concept imposes itself with regard to our findings and the rational that microdomain phase separation needs a process that stops growth and limits size of the domains [37]. In this context, we remind that 2D-crystals of AQP0 formed with sizes of several micrometers comprising ~200,000 AQP0 tetramers [28]; therefore, we conclude that AQP0 does not limit array size itself. The observation of rows of one, two, or three AQP0 tetramers width branching out of AQP0 arrays is strong evidence that the AQP0 tetramer was the minimal unit of assembly, in contrast to the recent proposal for the other array and junction forming aquaporin, AQP4, that square arrays consisted of higher-order complexes [38].

Taking into account the similar localization of connexons observed in both the young calf and in the adult sheep samples [23], we conclude that connexons play an essential role in the formation of junctional microdomains in lens membranes. In contrast, the supramolecular AQP0–connexon assembly is not directly AQP0 truncation dependent, as AQP0 truncation is less advanced in the young calf compared to the adult sheep tissue (see Fig. 2g). Well-organized junctional microdomains existed in young and mature tissue, in contrast to the pathological case, where connexons were absent.

As connexons ensure the ion, metabolite, and waste flux between neighboring cells, their absence is certainly responsible for the breakdown of the lens microcirculation system [2] and, hence for starvation, leading to lens opacification. The absence of connexons was already observed in senile human cataract [25]. Thus, it appears that connexons are the weak element of the microcirculation system on the molecular level; their degradation will induce a vicious circle of progressive breakdown of lens circulation of necessary compounds for cell and microdomain maintenance. The observed similarities between the diabetes II patient cataract, presented in this work, and the senile cataract membranes [25] evidence that the diabetes II pathology in this patient induced a degradation process that is similar to the age-dependent case, with the result of connexon degradation and malformation of AQP0 arrays.

Materials and methods

Sample preparation

The analyzed material originated from the right eye of a 78-year-old type II diabetes patient with a diabetes-induced cataract. The cataract lens was completely opaque (white) with amyloid depositions on the lens exterior. Preoperative

visual acuity of the right eye was 1/10, only light perception remaining. The patient suffered also from arterial hypertension. Under topical anesthesia (Tetracaïne chlorhydrate), cataract extraction was performed by phacoemulsification, in which the lens is emulsified with an ultrasound hand-piece, and aspirated from the eye. All extracted material was collected in a disposable recipient (connected to the fluid-control generator), which was transported on ice to the laboratory. The cataract debris, visible pieces of the lens tissue of millimeter size, was pelleted by centrifugation. Subsequently, the cells of the surgery debris were separated and broken using a homogenizer, followed by membrane washing and pelleting steps [5, 26].

For comparison, 20 calf lenses were dissected to remove the soft cortical tissue from the hard lens cores. These were pooled for cell breaking. Membranes were prepared from homogenized cell debris using the same protocol as applied for the cataract lens surgery debris.

Atomic force microscopy

Mica supports were immersed in 40 µl adsorption buffer (10 mM Tris–HCl, pH 7.4, 150 mM KCl, 25 mM MgCl$_2$). Subsequently, 3–5 µl of membrane solution were injected into the buffer drop. After ~30 min, the sample was rinsed with recording buffer (10 mM Tris–HCl, pH 7.4, 150 mM KCl). The AFM [10] was operated in contact mode at ambient temperature and pressure. Imaging was performed with a commercial Nanoscope-E AFM (Veeco, Santa Barbara, CA, USA) equipped with a 160-µm scanner (J-scanner) and oxide-sharpened Si$_3$N$_4$ cantilevers (length 100 µm; k=0.09 N/m; Olympus, Tokyo, Japan). For imaging minimal loading, forces of ~100 pN were applied, at scan frequencies of 4–7 Hz using optimized feedback parameters and manually accounting for force drift.

SDS-Polyacrylamide gel electrophoresis

Native and cataract lens membranes were incubated in sample buffer containing 1.5% SDS and 10% β-mercaptoethanol for 30 min at room temperature. Samples were loaded to SDS-PAGE (3% stacking and 12% resolving polyacrylamide gels) [39], run at 200 V and stained with silver or Coomassie Blue.

Mass spectrometry analysis–MALDI-TOF

Matrix-assisted laser desorption ionization (MALDI)-time-of-flight (TOF) analysis was performed on a mass spectrometer (Voyager-DE-PRO, Applied Biosystems, USA). Native cataract lens membranes were incubated in 80% formic acid (with or without 1% DDM) for 1 min at room temperature [25]. Then, 0.5 µl of sample were mixed with 2 µl of matrix solution (a-cyano-4-hydroxy-cinnamic acid,

50% acetonitrile/water 0.1 TFA) and deposited on the sample plate to dry. Acquisition of spectra of the cataract lens membrane proteins was performed in linear mode.

Data analysis

All image analysis of AFM topographs were performed using self-written routines [40] in the ImageJ image processing package [41] and MALDI-TOF spectra analyzed in IGOR PRO.

Structure modeling

A surface representation of the junctional AQP0 structure (2B6O [28]) was used for cross-correlation searches in the AFM topographs [40]. The spacing between and the rotational alignment of AQP0 of each cross-correlation peak was analyzed and averaged. The final structure model was assembled in PyMol [42].

References

1. Bloemendal H (1981) Molecular and cellular biology of the eye lens. Wiley, New York
2. Donaldson P, Kistler J, Mathias RT (2001) Molecular solutions to mammalian lens transparency. News Physiol. Sci. 16:118–123 DOI Electronic Resource Number
3. Andley U (2007) Crystallins in the eye: function and pathology. Prog Retin Eye Res 25:78–98 DOI Electronic Resource Number
4. Alcala J, Lieska N, Maisel H (1975) Protein composition of bovine lens cortical fiber cell membranes. Exp Eye Res 21:581–595 DOI Electronic Resource Number
5. Gonen T, Cheng Y, Kistler J, Walz T (2004) Aquaporin-0 membrane junctions form upon proteolytic cleavage. J Mol Biol 342:1337–1345 DOI Electronic Resource Number
6. Fleschner C, Cenedella R (1991) Lipid composition of lens plasma membrane fractions enriched in fiber junctions. J Lipid Res 32:45–53 DOI Electronic Resource Number
7. Shiels A, Bassnett S (1996) Mutations in the founder of the MIP gene family underlie cataract development in the mouse. Nature Genet. 12:212–215 DOI Electronic Resource Number
8. www.WHO.int (2007) Diabetes Programme
9. Wild S, Roglic G, Green A, Sicree R, King H (2004) Global prevalence of diabetes: estimates for the year 2000 and projections for 2030. Diabetes Care 27:1047–53 DOI Electronic Resource Number
10. Binnig G, Quate CF, Gerber C (1986) Atomic force microscope. Phys Rev Lett 56:930–933 DOI Electronic Resource Number
11. Schabert FA, Henn C, Engel A (1995) Native *Escherichia coli* OmpF porin surfaces probed by atomic force microscopy. Science 268:92–94 DOI Electronic Resource Number
12. Seelert H, Poetsch A, Dencher NA, Engel A, Stahlberg H, Müller DJ (2000) Proton powered turbine of a plant motor. Nature 405:418–419 DOI Electronic Resource Number
13. Scheuring S, Seguin J, Marco S, Levy D, Robert B, Rigaud J-L (2003) Nanodissection and high-resolution imaging of the *Rhodopseudomonas viridis* photosynthetic core-complex in native membranes by AFM. Proc Natl Acad Sci 100:1690–1693 DOI Electronic Resource Number
14. Scheuring S, Sturgis JN, Prima V, Bernadac A, Lévy D, Rigaud J-L (2004) Watching the photosynthetic apparatus in native membranes. Proc Natl Acad Sci USA 101:11293–11297 DOI Electronic Resource Number
15. Scheuring S, Busselez J, Levy D (2005) Structure of the dimeric PufX–containing core complex of *Rhodobacter blasticus* by in situ AFM. J Biol Chem 180:1426–1431 DOI Electronic Resource Number
16. Scheuring S, Sturgis JN (2005) Chromatic adaptation of photosynthetic membranes. Science 309:484–487 DOI Electronic Resource Number
17. Gonçalves RP, Bernadac A, Sturgis JN, Scheuring S (2005) Architecture of the native photosynthetic apparatus of *Phaeospirillum molischianum*. J Struct Biol 152:221–228 DOI Electronic Resource Number
18. Scheuring S, Gonçalves RP, Prima V, Sturgis JN (2006) The photosynthetic apparatus of *Rhodopseudomonas palustris*: structures and organization. J Mol Biol 358:83–96 DOI Electronic Resource Number
19. Bahatyrova S, Frese RN, Siebert CA, Olsen JD, Van Der Werf KO, van Grondelle R, Niederman RA, Bullough PA, Hunter CN (2004) The native architecture of a photosynthetic membrane. Nature 430:1058–1062 DOI Electronic Resource Number
20. Fotiadis D, Liang Y, Filipek S, Saperstein DA, Engel A, Palczewski K (2003) Atomic-force microscopy: Rhodopsin dimers in native disc membranes. Nature 421:127–128 DOI Electronic Resource Number
21. Buzhynskyy N, Sens P, Prima V, Sturgis JN, Scheuring S (2007) Rows of ATP synthase dimers in native mitochondrial inner membranes. Biophys J 93:2870–2876 DOI Electronic Resource Number
22. Gonçalves RP, Buzhynskyy N, Prima V, Sturgis JN, Scheuring S (2007) Supramolecular assembly of VDAC in native mitochondrial outer membranes. J Mol Biol 369:413–418 DOI Electronic Resource Number
23. Buzhynskyy N, Hite RK, Walz T, Scheuring S (2007) The supramolecular architecture of junctional microdomains in native lens membranes. EMBO Reports 8:51–55 DOI Electronic Resource Number
24. Scheuring S, Buzhynskyy N, Jaroslawski S, Gonçalves RP, Hite RK, Walz T (2007) Structural models of the supramolecular organization of AQP0 and connexons in junctional microdomains. J Struct Biol 160:385–394 DOI Electronic Resource Number
25. Buzhynskyy N, Girmens J-F, Faigle W, Scheuring S (2007) Human cataract lens membrane at subnanometer resolution. J Mol Biol 374:162–169 DOI Electronic Resource Number
26. Gonen T, Sliz P, Kistler J, Cheng Y, Walz T (2004) Aquaporin-0 membrane junctions reveal the structure of a closed water pore. Nature 13:193–197 DOI Electronic Resource Number
27. Harries WE, Akhavan D, Miercke LJ, Khademi S, Stroud RM (2004) The channel architecture of aquaporin 0 at a 2.2-A resolution. Proc Natl Acad Sci 101:14045–14050 DOI Electronic Resource Number
28. Gonen T, Cheng Y, Sliz P, Hiroaki Y, Fujiyoshi Y, Harrison SC, Walz T (2005) Lipid–protein interactions in double-layered two-dimensional AQP0 crystals. Nature 438:633–638 DOI Electronic Resource Number

29. Unger V, Kumar N, Gilula N, Yaeger M (1999) Three-dimensional structure of a recombinant gap junction membrane channel. Science 283:1176–1180 DOI Electronic Resource Number

30. Riley M, Harding J, Kilby G, Truscott R, Aquilina A, Sheil M (1996) Molecular masses of gamma-crystallins. Ophthalmic Res 28:131–135 DOI Electronic Resource Number

31. Fan J, Donovan A, Ledee D, Zelenka P, Fariss R, Chepelinsky A (2004) gammaE-crystallin recruitment to the plasma membrane by specific interaction between lens MIP/aquaporin-0 and gammaE-crystallin. Invest Ophthalmol Vis Sci 45:863–871 DOI Electronic Resource Number

32. Yu X, Jiang J (2004) Interaction of major intrinsic protein (aquaporin-0) with fiber connexins in lens development. J Cell Science 117:871–880 DOI Electronic Resource Number

33. Zampighi G, Simon SA, Robertson JD, McIntosh TJ, Costello MJ (1982) On the structural organization of isolated bovine lens fiber junctions. J. Cell Biol. 93:175–189 DOI Electronic Resource Number

34. Zampighi GA, Eskandari S, Hall JE, Zampighi L, Kreman M (2002) Micro-domains of AQP0 in lens equatorial fibers. Exp. Eye Res. 75:505–519 DOI Electronic Resource Number

35. Ball LE, Little M, Nowak MW, Garland DL, Crouch RK, Schey KL (2003) Water permeability of C-terminally truncated aquaporin 0 (AQP0 1–243) Observed in the Aging Human Lens. Invest Ophthalmol Vis Sci 44:4820–4828 DOI Electronic Resource Number

36. Gonen T, Hite RK, Cheng Y, Petre BM, Kistler J, Walz T (2008) Polymorphic assemblies and crystalline arrays of lens tetraspanin MP20. J Mol Biol 376:380–392 DOI Electronic Resource Number

37. Fielding C (2006) Lipid rafts and caveolae: from membrane biophysics to cell biology. Wiley, Weinheim, Germany

38. Sorbo JG, Moe SE, Ottersen OP, Holen T (2008) The Molecular composition of square arrays. Biochemistry 47:2631–2637 DOI Electronic Resource Number

39. Laemmli UK (1970) Cleavage of structural proteins during assembly of the head of bacteriophage T4. Nature 227:680–685 DOI Electronic Resource Number

40. Scheuring S, Boudier T, Sturgis JN (2007) From high-resolution AFM topographs to atomic models of supramolecular assemblies. J Struct Biol 159:268–276 DOI Electronic Resource Number

41. Rasband WS (1997–2005) ImageJ. U.S. National Institutes of Health, Bethesda, Maryland, USA, http://rsb.info.nih.gov/ij/ Resource Number

42. DeLano WL (2002) The PyMOL Molecular Graphics System, http://www.pymol.org. Resource Number